ADVANCED INTELLIGENT SYSTEMS
Open Access
www.advintellsyst.com

Electronic-Free Particle Robots Communicate through Architected Tentacles

Xinyi Yang, Bohan Wang, Víctor Riera Naranjo, Minghao Guo, Olivia Rivera, Leonid Sopizhenko, Shucong Li, William Freeman, Wojciech Matusik,* and Bolei Deng**

Communication among particle robots is crucial for developing swarm intelligence. Current particle robots rely entirely on electronic communication systems, requiring a sensor to receive signals, a transducer to send signals, a processor to process them, and a battery to power the system. In this work, an alternative, electronics-free communication strategy for particle robots is introduced via physical contact between their architected tentacles. Instead of relying on a central controller, the communication protocols are embodied in the geometrical outlines of these tentacles and can be further tuned with external vibrations. Separated particles can interlock under external pressure to form stable clusters resembling "solids," or vaporize into "gas" by spontaneously repelling one another. Surrogate simulation tools have been developed to guide the design of these robots, enabling the inverse design of particle geometries for programmable interlocking and repulsion. Based on these basic communication schemes, particle robots can achieve a range of functionalities through collective behavior, including fast, sequential, and hierarchical deployment, locomotion, and coordinated group navigation. Finally, this contact-based communication concept is extended to particles with different shapes, hybrid particle interactions, 3D particles, and microscale particle robots.

1. Introduction

Swarm intelligence,[1,2] a captivating natural phenomenon, involves decentralized systems interacting with their environment and each other to achieve collective behavior.[3–5] Two individual agents, such as animals, can exhibit a range of simple behaviors, including repelling, attracting, following, aligning, and collaborating, which contribute to more complex global swarm behaviors,[6] such as flocking,[7–9] self-organization,[10–13] and decentralized control.[14,15] To replicate these behaviors, researchers have developed particle robotics, also known as group robots.[16–19] This development empowers robots with adaptability, enabling them to collectively adjust their behavior in response to changes in their environment or goals.[20] Particle robots also possess enhanced overall robustness, as they can withstand individual failures, with the overall behavior distributed across many agents.[21,22] Additionally, the system of particle robots is scalable, with the collective behavior remaining effective regardless of the group size.[23,24] The critical aspect of building these systems lies in establishing effective communication and interactions among individual units,[3] which are essential for swarm intelligence to emerge. Current man-made group robots primarily rely on electronic components—such as signal generators, receivers, processors, and power supplies[25–28]—to dictate how a particle should interact with its neighbors. Consequently, a significant portion of the space, cost, and energy in these systems is dedicated to enabling electronic communication and interaction. The physical contacts between particle robots, such as normal force and friction, offer a natural means of communication.[29,30] However, these passive interactions do not inherently encode information, making them insufficient for providing meaningful interactions necessary for swarm intelligence.

In recent years, the realm of mechanical metamaterials or architected materials[31–33] has realized unprecedented material properties, such as negative Poisson ratios,[34–36] multi-

X. Yang, V. R. Naranjo, L. Sopizhenko, B. Deng
Daniel Guggenheim School of Aerospace Engineering
Georgia Institute of Technology
Atlanta 30332, USA
E-mail: bolei.deng@gatech.edu

The ORCID identification number(s) for the author(s) of this article can be found under https://doi.org/10.1002/aisy.202500151.

DOI: 10.1002/aisy.202500151

B. Wang
School of Computing
National University of Singapore
117417, Singapore

B. Wang, M. Guo, O. Rivera, W. Freeman, W. Matusik
Computer Science and Artificial Intelligence Laboratory
Massachusetts Institute of Technology
Cambridge 02139, USA
E-mail: billf@mit.edu; wojciech@mit.edu

S. Li
School of Materials Science and Engineering
Georgia Institute of Technology
Atlanta 30332, USA

stability,[37,38] and phononic bandgaps.[39–41] These exotic properties are induced and governed by their geometries rather than chemical compositions.[42–45] In other words, one can engineer the geometry of their meso-structures to achieve certain desired mechanical properties. Drawing a parallel, if we consider each particle robot as a fundamental building block akin to a unit in a metamaterial,[46] an enticing question arises: Can we strategically design the geometrical outlines of these particle robots to facilitate programmable interactions, which ultimately culminate in swarm intelligence?

In this article, we propose a contact-based communication scheme between particle robots that operates without electronic components. Their communications protocols are embodied in their architected tentacles, whose multi-stable interactions allow for stable locking and unlocking between neighboring particles. Additionally, these interactions can be modulated by small-amplitude vibrations, which can release stored elastic energy within the tentacles and cause the interlocked particles to spontaneously repel each other at high speeds. The stability of interlocking, the timing of repulsion, and the relative repelling velocity can be precisely programmed by adjusting the geometrical design of the tentacles and the characteristics of the vibrations. These straightforward and controllable interactions foster a degree of swarm intelligence within the robot group, giving rise to capabilities like rapid, sequential, and hierarchical deployment, as well as the formation of spontaneous protective shells and group navigation.

2. Results

2.1. Contact-Based Interaction

In nature, various animals employ tentacles to exchange information with other individuals and their surrounding environment. For example, mosquitoes detect the wing beats of potential mates with their tentacles, which is crucial for reproduction.[47,48] Similarly, viruses, even though they cannot move by themselves, rely on tentacle-like structures to precisely attach and interact with host cells, enabling effective communication at a molecular level.[49–51] Inspired by this, we propose particle robots that communicate with each other through the physical contact between the tips of their tentacles (see **Figure 1**A). To ensure isotropic interactions in arbitrary directions, we designed 2D particle robots with a circular shape and evenly distributed tentacles (see Supplementary materials, Session S1). These particles are fabricated by laser cutting 1/8-inch-thick acrylic plates (see Supplementary materials, Session S2). During testing, the particles are positioned on a 1/2-inch-thick acrylic plate serving as the testing substrate. When two robots come within a specific center-to-center distance, their tentacles deform to grip each other. The normal force and friction between the tentacles enable a stable locking mechanism between two particles (see Figure 1B). In our system, the normal forces that govern frictional locking are generated by elastic deformation of the tentacles, rather than by the gravitational weight of the particle robots. Moreover, recent research suggests that small amplitude and high-frequency vibrations can be used to modify the

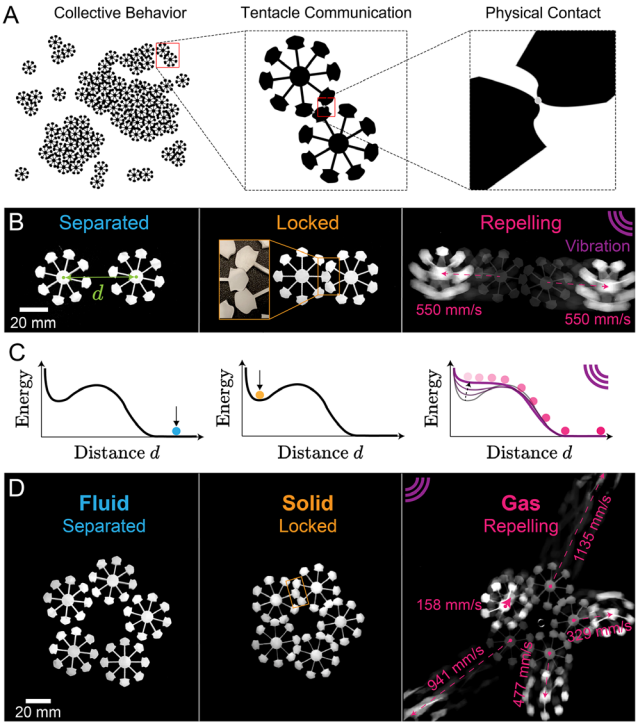

Figure 1. A) Electronic-free particle robots exhibit collective behaviors (Left); individuals communicate through physical contact of tentacles (Middle); communication protocols are embodied in the geometric design of tentacle tips (Right). B) Three states of particle robots: Separated, interlocked, and repelling. (Left) When two particle robots are brought in close proximity below a certain center-to-center distance, they can stably interlock through mechanical contacts using their tentacles; (Middle) When the vibration is triggered, two particle robots repel each other at a certain speed; (Right) Two particle robots finally reach a separate state. C) Energy landscape for each state shown above. D) When several particle robots collectively interact, they can transition from a liquid phase (Left), where the particles remain separated, to a solid phase (Middle), forming a locked block, and finally, to a gaseous phase (Right), where all particles have kinetic energy.

contact properties between two interfaces.[52–55] To explore the effect of vibrations on locked particles, we introduce a vibration to the substrate with an amplitude $A_v = 0.1$ mm and frequency $f_v = 100$ Hz by attaching a Modal Shaker K2025E01 to the bottom of the substrate (see Supplementary materials, session S3). When subjected to such small-amplitude vibrations, the interlocked particles spontaneously repel each other at a relative velocity of 550 mm s^{-1} (see Figure 1B and Movie S1). This mesmerizing lock-and-repel behavior stems from a unique interaction energy landscape between the particles. With carefully designed tentacle geometry, the particles can exhibit two stable states: separated and locked. Normally, transitioning from the locked to the separated state requires additional energy to overcome the energy barrier. However, the applied vibration alters the equivalent interaction energy landscape from bistable to monostable (see Figure 1C). Consequently, without an energy barrier, the particles spontaneously disengage without external force, and the elastic energy stored in their tentacles is converted into kinetic energy. Furthermore, this interaction behavior extends beyond just two

particles; it can be scaled up to involve multiple particle robots. When they collectively interact, they can transition from a liquid phase, where the particles remain separated, to a solid phase, forming a locked block, and finally, to a gaseous phase, where all particles possess kinetic energy (see Figure 1D and Movie S2).

2.2. Role of Vibration

In order to figure out how small-amplitude vibration controls the repelling process, we take a closer look at the repelling process in **Figure 2**. At $t = 0$ s, the shaker is turned on delivering a vibration with amplitude $A_v = 0.1$ mm and frequency $f_v = 100$ Hz perpendicular to the substrate, where A_v and f_v are measured by an accelerometer attached to the substrate (see Supplementary materials, Session S3). In the beginning, two particles stay locked while the vibration is on. At $t = 1.86$ s, two particles instantly repel each other and travel in opposite directions (see Figure 2A). To get a more quantitative understanding, in Figure 2B, we monitor the center-to-center distance d between two particles as a function of time t by tracking the green dots on each particle. The distance d first remains constant from 0 to 1.86 s corresponding to the locked state, quickly increases from 1.86 to 2.04 s where particles repel each other at a relative velocity of $v_r = 974$ mm s^{-1}, and finally after 2.04 s particles slow down and come to a rest separation. It is crucial to understand why the particles do not instantly repel each other when the substrate begins to vibrate; instead, there is a loading time of $t_l = 1.86$ s before repulsion starts. To investigate this, we examine the loading period by simulating the z-directional trajectory of a particle resting on the vibrating substrate. Since the substrate is connected to a shaker, its movement is confined to the z direction and follows the sinusoidal function $z(t) = A_v \sin(2\pi f_v t)$. At $A_v = 0.1$ mm and frequency $f_v = 100$ Hz, the substrate achieves a maximal acceleration of $\approx$39.5 m s^{-2}, noticeably exceeding gravitational acceleration ($g = 9.8$ m s^{-2}). As a result, during each vibration cycle, the particle experiences lift-off from the platform, followed by a fall and collision with the platform. The intensity of these weak collisions is equivalent to dropping the particle from a height of 0.1–0.2 mm. Hundreds of such micro-collisions occur before the two particles begin to repel each other at $t = t_l$. Each micro-collision subtly alters the contact points between the tentacles, and the cumulative effect of these shifts eventually disengages the interlocking (see Supplementary Materials, Section S4A for a detailed analysis of micro-collisions and the energy transfer efficiency of this process).

We then repeat the experiment with increasing vibration amplitude from $A_v = 0.05$ to 0.25 mm, resulting in decreasing loading time t_l (see Figure 2D). Under a constant frequency f_v, a higher amplitude A_v results in a greater maximal velocity v_{max} during each vibration cycle, expressed by $v_{max} = 2\pi f_v A_v$. Consequently, particles are lifted higher from the substrate, leading to stronger collisions upon return. These more intense collisions reduce the number of impacts required for the particles to start repelling each other, therefore shortening the loading time t_l. We developed a theoretical model to capture the energy transfer mechanism between the vibrating platform and the particles, enabling a good prediction of the loading

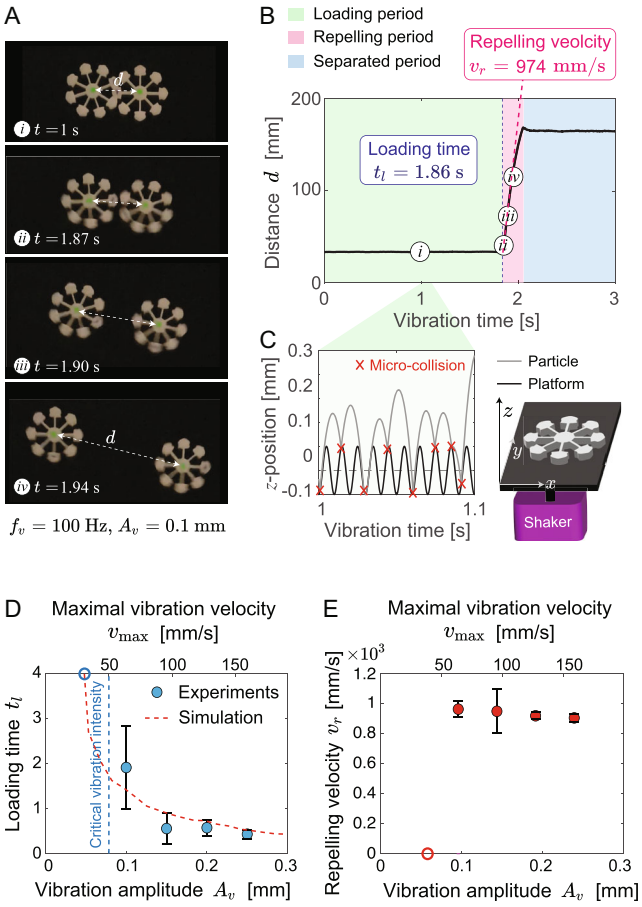

Figure 2. A) The states and corresponding response time for two particle robots under external vibration with amplitude $A_v = 0.1$ mm and frequency $f_v = 100$ Hz. B) Vibration time and the displacement curve between two particle robots. Three distinct periods are shown during the vibration: the loading period, the repelling period, and the separated period. C) Relationship between the vibration time and the displacement of the tested particle robot (gray line) and the testing platform (black line). The red crosses represent the micro-collision point between the particle and the platform. D) Comparison of loading time (t_l) as a function of vibration amplitude (A_v), with experimental data (blue dots) aligning with theoretical predictions (dashed red line). E) The particles repel each other at an almost constant repelling velocity for different amplitudes.

time t_l (see red dashed line in Figure 2D; for details, refer to Supplementary Materials, Session S4). While the intensity of the micro-collision is directly proportional to the maximal vibration velocity v_{max} of the substrate, the frequency of such collisions is related to the vibration frequency f_v. It is important to point out that there is a threshold collision intensity below which the particles will not repel each other, regardless of how many micro-collisions transpire. Above this threshold, the particles repel each other after a certain loading time t_l at an almost constant repelling velocity v_r irrespective of the collision intensity or frequency (see Figure 2E). This is because the kinetic energy of the particles originates from the potential energy stored in their tentacles accumulated during the locking process, which is unrelated to the releasing mechanism. As will be discussed in the next section, both the released energy and

the vibration threshold, or in simpler terms, the ease with which vibrations can separate the particles, are completely programmable through the geometrical design of their tentacles.

2.3. Geometry Governed Interaction

As mentioned in the previous section, the interaction between two particles can be controlled by the geometry of their tentacles (see Supplementary materials, Session S1). To delve deeper into the mechanics of these interactions, we performed a static compression test on two particles (see Supplementary materials, Session S3A). As depicted in **Figure 3**A, the particles are pushed together to engage and pulled apart to disengage. Specifically, one tentacle is inserted and removed between two others, and the resulting force f is measured as a function of the center-to-center distance d. This test was conducted both experimentally (see Supplementary materials, Session S3) and numerically (see Supplementary materials, Session S4); in our numerical model, the friction coefficient between tentacles is set to $\mu = 0.3$, a typical value for acrylics. In Figure 3B, we present a side-by-side comparison of both numerical results (solid line) and experimental findings (triangular markers), which closely align and thereby confirm the accuracy of our numerical model. The initial negative segment of the f-d curve during the separation process, highlighted by the yellow region in Figure 3B, represents the locking energy required to separate two interlocked particles. When the substrate starts to vibrate, we hypothesize that the high-frequency micro-collisions effectively reduce the friction coefficients μ between the tentacles. To simulate the role of vibration, we conducted separation tests at varying μ values and recorded the force responses f. As shown in Figure 3B, lower μ values lead to decreased locking energy, and at a critical friction coefficient of $\mu_c = 0.084$, the locking energy drops to zero. This indicates that when $\mu < \mu_c$, nothing prevents the particles from separating, allowing them to

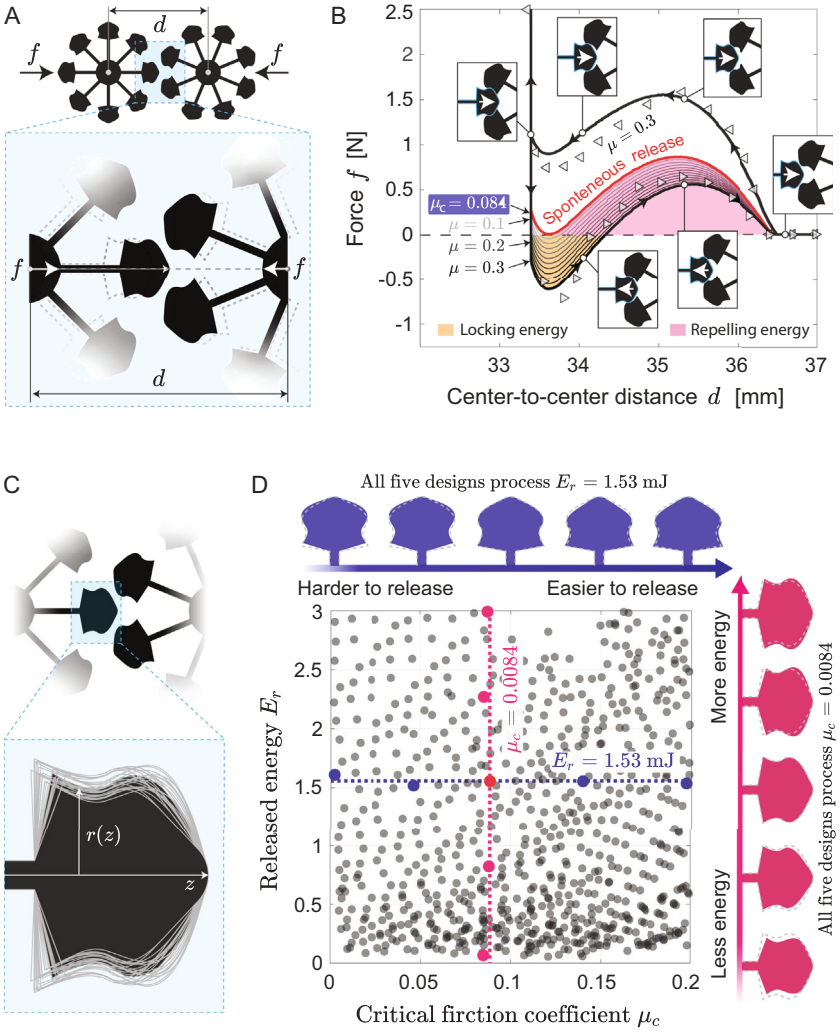

Figure 3. A) In the static compression tests simulation, one tentacle is inserted into then separated from another two tentacles between two tentacles to get the corresponding force and displacement (See SI, Session S3 and Session S4). B) The response force f is measured as a function of center-to-center distance d. It shows the locking energy required to separate two interlocked particles. C) 1500 meaningful tentacle geometries are generated to test releasing energy E_r and critical friction coefficient μ_c. D) Numerical simulation of 1500 designs in the phase diagram of E_r and μ_c.

spontaneously detach from each other. During this detachment process, the force exerts in the direction of separation transforming the energy stored in the tentacles into kinetic energy. This quantity can be calculated by integrating the corresponding section of the $f - d$ curve at $\mu = \mu_c$ highlighted in the pink region of Figure 3B. From this static test, we can derive the two critical parameters that describe the particle interactions: the critical friction coefficient μ_c and repelling energy E_r. While μ_c indicates the ease of particle separation using vibration, E_r quantifies the kinetic energy released.

Next, we explore how the critical friction coefficient (μ_c) and release energy (E_r) can be precisely controlled through the geometry of the tentacles. We begin by systematically generating 1500 distinct tentacle geometries (see Figure 3C and Supplementary materials, Session S1). For each design, we perform numerical tests illustrated in Figure 3B and extract the corresponding μ_c and E_r. As shown in Figure 3D, the results expand the μ_c-E_r performance space, indicating that we can inversely design the tentacle geometries tailored to any desired μ_c and E_r. To illustrate how tentacle shape affects interaction characteristics, we select five tentacle geometries with identical release energy ($E_r = 1.53$ mJ, as depicted in Figure 1 and 2), but with progressively increasing μ_c, meaning they are easier to separate by vibrations (see blue tentacles at the top of Figure 3D). Geometrically, the tentacles to the left feature a wider head for a more stable lock, while those on the right have sharper heads for a less stable lock. Additionally, we present five tentacle designs with increasing E_r while maintaining a constant $\mu_c = 0.084$, demonstrating that wider tentacles, which bend more during locking, store more energy (see magenta tentacles on the right in Figure 3D). Although we only investigate the effect of the head shape of tentacles, other parameters, such as the thickness and length of the beam, and number of tentacles, also have a significant impact on E_r and μ_c. These parameters can be further tailored for specific tasks.

2.4. Particle Robots

The programmable interactions between particle robots, such as locking and repelling, enable unique communication patterns that can be scaled up to larger systems for various group functionalities.

2.4.1. Fast Deployment

A natural extension of the repelling of two particles is the "vaporization" of a group of interlocked particles. Thanks to their radially symmetric shapes, particles can be assembled amorphously into a group of any size. Under external vibration, the potential energy stored in the tentacles is transformed into kinetic energy of the particles, allowing the initially clustered particles to deploy rapidly into the environment (see **Figure 4**A). Since neighboring particles tend to move away from each other, the final deployed particles are often distributed sparsely and evenly (see Movie S3 and Movie S4).

2.4.2. Sequential Deployment

Employing particles with different μ_c values allows for controlled sequential deployment by tuning the amplitude of vibration. Specifically, we select two types of particles: one more resistant to vibration ($\mu_c = 0.084$) and the other less resistant ($\mu_c = 0.14$). They are assembled into two distinct clusters (see Figure 4B). At a vibration amplitude of $A_v = 0.05$ mm, the less resistant group dissembles; the more resistant group remains interlocked until the amplitude increases to 0.1 mm. This sequential deployment is fully controlled by external vibration and is effective for any cluster configuration (see Movies S5 and S6).

2.4.3. Hierarchical Deployment

Particles with different μ_c values can be assembled into a single cluster to achieve hierarchical deployment. As shown in Figure 4C, the outer sections of the cluster, which are connected to the core through weaker particles, detach from the core at a lower vibration amplitude ($A_v = 0.05$ mm). These detached sections, as well as the core, then further disintegrate under a higher amplitude ($A_v = 0.1$ mm, see Movie S7). Such hierarchical deployment allows for more precise delivery of particle robots into complex spaces, where subgroups can initially navigate through narrow tunnels and subsequently deploy further. In fact, it would also be possible to encode more complex collective behaviors by constructing a group that contains many distinct particle designs. Each particle design would have its own unique "fingerprint," resulting in different interactions between various types of particles.

2.4.4. Active Protective Shells

Additionally, particles can form active protective shells which can "vaporize" on demand. The kinetic energy released by the shell can clear surrounding obstacles, creating a safer environment for the target object (see Figure 4D, Movie S8). Protective shells can also form spontaneously around a target object when subjected to external pressure. In such cases, tentacle entanglement in high-density assemblies can lead to more complex locking scenarios; this issue is addressed by increasing the number of tentacles from 8 to 15, as detailed in Supplementary Figure S7, Supporting Information.

2.4.5. Directional Locomotion

Recent work have demonstrated that vibration can enable locomotion through carefully designed surfaces, allowing for complex motion patterns such as rotation[56] and translation.[57] This paves the way for integrating crawling functionalities into our particle systems. To demonstrate this, we 3D print new types of particles with sawtooth-like bases. Due to the asymmetric shape of the sawtooth, small-amplitude vibrations cause the particles to slowly crawl in a predetermined direction (see Figure 4E and Movie S9, where the intended movement direction is indicated by an arrow on top of each particle). Initially, two connected particles crawl in the direction of their arrows when subjected to low-level vibrations. As the vibration amplitude is increased

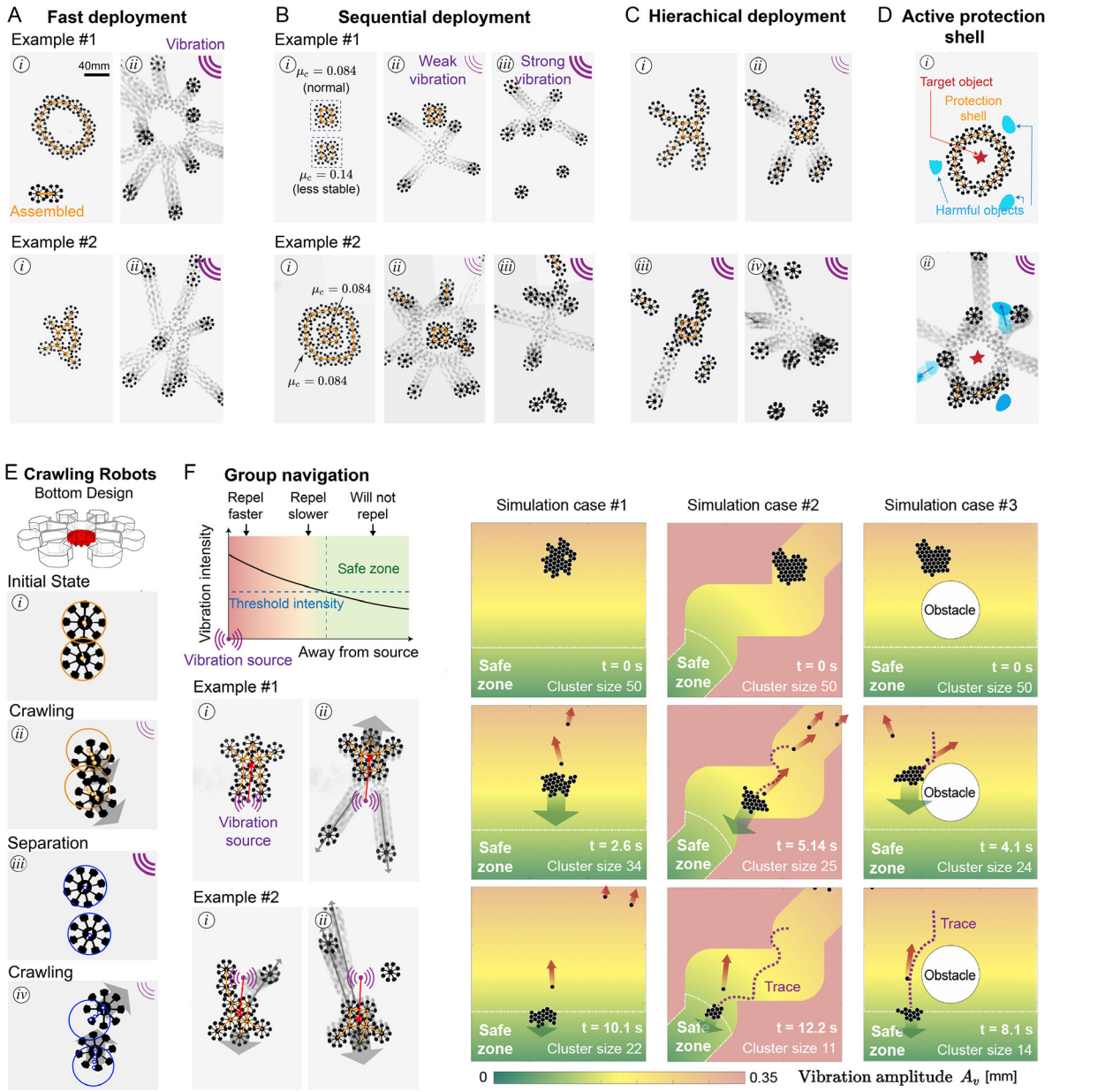

Figure 4. Group Functionalities of Particle Robot Systems. A) Fast Deployment: Clustered particle robots can rapidly deploy into the environment within seconds. B) Sequential Deployment: Multiple clusters of particle robots with different μ_c values can be triggered sequentially. C) Hierarchical Deployment: A single cluster of particle robots with varying μ_c values can achieve hierarchical deployment. D) Protective shells: When certain vibration is triggered, the particle robots can repel each other to release the kinetic energy, thus cleaning up harmful objects around the target object. E) Particle robots achieve directional crawling through the modification their bottom surfaces. During the experiment, the center points of the particle robots were tracked, and their trajectories are plotted in Figure 4E. Orange dots represent the paths before the actuation vibration is triggered, while blue dots show the paths after the vibration is triggered. F) Group Navigation: particle robots can exhibit swarm intelligence by navigating away from hostile environments.

beyond a critical threshold, the particles separate and each one of them continues to crawl independently in their respective intrinsic directions.

2.4.6. Group Navigation

Finally, we demonstrate how mechanically based particle robots can exhibit swarm intelligence, such as navigating away from hostile environments. As previously discussed in Figure 2D, stronger vibrations take less loading time for particles to separate. When the vibration is applied at a single point, its intensity diminishes with distance, causing particles closer to the source to repel first (see Figure 4F, Movie S10 and S11). Due to momentum conservation, this process continuously propels the main cluster away from the source until it reaches a safe distance, where the vibration intensity becomes too weak to trigger particle

repelling. We have developed a surrogate model to simulate the swarm behavior of large clusters (see Simulation Case#1 in Figure 4F). The entire group consistently navigates away from the vibration source by sacrificing a few peripheral individuals—a classic demonstration of swarm intelligence. Further simulation results reveal that by leveraging this minimalistic communication mechanism between two particles, a robot cluster can exhibit complex group behaviors such as navigating intricate pathways (Case #2) and circumventing obstacles (Case #3). While the experimental results focus on swarms of up to 12 particles, larger-scale numerical simulations with up to 150 particles confirm that the system remains stable and becomes increasingly robust and fault-tolerant as swarm size increases (see Supplementary Section S4C, Movie S12 and Figures S13–S20, Supporting Information).

2.5. Extension to Different Configurations, Mixed Pairs and 3D Particle

The concept of programming interactions between particle robots using tentacles can be further extended to different configurations, interaction matrices and 3D scenarios.

2.5.1. Different Geometries and Configurations

The communication between particles is governed by their tentacle design, which allows the particle robots to be adapted to various geometries and configurations. We designed two additional particle types—square and hexagonal—with tentacles along their edges. Experiments on the vibration platform (**Figure 5**A, Movie S13)

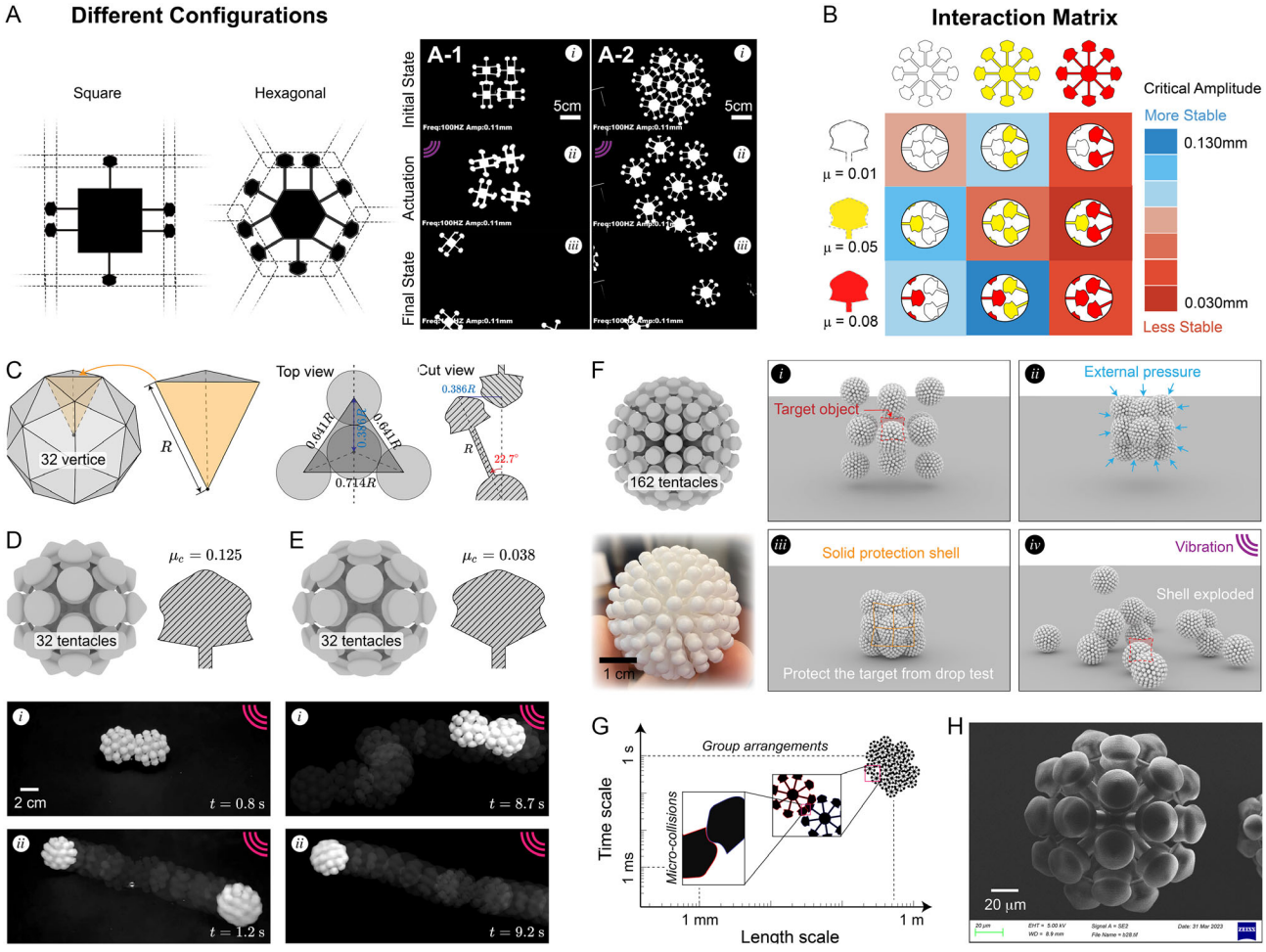

Figure 5. Extension to different configurations, mixed pairs, and 3D particles. A) Locking and repelling behaviors of particle robots with square and hexagonal configurations. B) Interaction matrix summarizing the critical actuation amplitudes for three particle robots with varying critical friction coefficients ($\mu_c = 0.01, 0.05, 0.08$), highlighting distinct interaction profiles for each interaction scenario. C) Design of 3D particle robots with 32 tentacles. D) and E) Two particle robots with different μ_c values and their corresponding releasing behaviors are shown. D) The less stable particle with $\mu_c = 0.125$ takes 1.2 s to repel, while E) the more stable particle with $\mu_c = 0.038$ pair requires 9.2 s to separate. F) Design of 3D particle robots with 162 tentacles, along with a simulation of multiple particle robots demonstrating their functionality as protective shells. G) The particle robot systems, both 2D and 3D versions, feature dual spatial and temporal dimensions. H) Microscale particle robots fabricated using IP-S resin via Nanoscribe. This material provides high resolution and mechanical stability, making it ideal for intricate designs at the micrometer scale.

revealed that, unlike circular particles, which pack randomly as marbles, square, and hexagonal particles align more systematically, resembling floor tiles. This tighter, more structured packing offers potential advantages for applications requiring precise arrangements.

2.5.2. Interaction Matrix

We also explored interactions between distinct particle designs by fabricating and testing the interaction between three types of robots with different critical friction coefficients: $\mu_c = 0.01$ (white, most stable), 0.05 (yellow, less stable), and 0.08 (red, least stable). These variations result in $3 \times 3 = 9$ unique one-on-one locking scenarios, as shown in Figure 5B and Movie S14. We evaluated the critical vibration amplitude for all nine cases by gradually increasing the vibration amplitude until the particles spontaneously repelled each other, under a constant vibration frequency of $f_v = 100$ Hz. Figure 5B shows the experimental results for all nine cases in an interaction matrix, where each element represents a distinct communication scheme. Along the diagonal, the critical vibration amplitudes for same-particle locking cases are observed: the most stable $\mu_c = 0.01$ (white) particles require 0.091 mm to separate, while the least stable $\mu_c = 0.08$ (red) particles need only 0.040 mm. These results align with the predicted critical friction coefficients. The off-diagonal terms reveal intriguing behaviors. The matrix is asymmetric; for example, a red particle's tentacle inserted between two white tentacles (bottom left) requires 0.11 mm to separate, whereas a white particle's tentacle between two red tentacles is less stable, needing only 0.04 mm. Furthermore, cross-locking stability can exceed that of either particle alone, demonstrating unique characteristics not defined by individual properties. This cross-locking behavior significantly increases system complexity, as 10 distinct particle types would yield 100 unique one-on-one interaction scenarios, not to mention the complexity of multi-particle interactions. Each particle's shape serves as a "fingerprint," offering opportunities for engineering more sophisticated group behaviors.

2.5.3. 3D Particles

Similar to 2D particles, 3D particles should have tentacles evenly distributed on the surface of a sphere to ensure omnidirectional interactions (see Supplementary materials, Session S1). In 2D, one tentacle inserts between two others; while in 3D, a tentacle inserts into a triangle formed by three others (see Figure 5C). Unlike 2D, where regular polygons can have any number of vertices, 3D is limited to only five types of regular polyhedra. The icosahedron, with the most triangular faces, still only has 12 vertices—too few for 3D particles to effectively lock with multiple neighbors in 3D space. To overcome this, we relax the requirement for evenly distributed tentacles, instead ensuring they form identical triangles. This approach ensures uniform interaction by making every insertion identical since the particle's surface possesses only one type of triangle. With this constraint, we are able to find a suitable polyhedron with 32 vertices. The 3D tentacles are formed as a solid of revolution from the 2D tentacle design (Figure 5C). During insertion, all three tentacles on a triangle are pushed and deformed equally away from the circumcenter, mirroring the 2D interaction mechanism. In a cut view, this interaction closely resembles the 2D case but at a specific angle—in this instance, 22.7 for the 32-vertex configuration. Following this idea, we design two types of 3D particle robots: one less stable against vibration ($\mu_c = 0.125$, see Figure 5D) and a more stable one ($\mu_c = 0.038$, see Figure 5E). The 3D particles are fabricated using selective laser sintering with Nylon 12 in a natural white color. Both designs achieve stable locking, but under external vibration ($A_v = 0.2$ mm), the less stable particles repel each other at $t = 1.2$ s, while the more stable ones resist longer, repelling at $t = 9.2$ s (see Figure 5D and E, movie S15 and S16). We can further expand our design to include 3D particles with up to 162 tentacles, accommodating more complex neighboring interactions. In Figure 5F, we use full numerical simulations (see Supplementary materials, Session S4, and Movie S17) to demonstrate their functionality as protective shells. Surrounding a target object, the particles quickly form a solid protective shell under external pressure, effectively shielding the target from a drop test without disintegration. This shell can then be disintegrated by external vibration, releasing the enclosed target.

3. Conclusion

In this article, we introduce an innovative particle robot system that, instead of relying on complex electronic components, leverages geometric design and physical contact to achieve simple communication (locking and repelling). Based on this one-to-one interaction protocol, a group of contact-based particles can exhibit various collective behaviors that are controllable by vibrations. Since the intelligence of these robotics is fully embodied in their geometrical outlines, hundreds of these particle robots can be easily fabricated using laser cutting (2D particle robots) or 3D printing (3D particle robots) within an hour and without the need for assembly, significantly reducing manufacturing complexity and time. The contact-based communication proposed in our project can also be combined with conventional electronic devices, leading to more powerful particle robots with more complex and advanced features.

Additionally, our study of particle robots unveils a complex interplay of mechanics across both spatial and temporal dimensions. The system features dual multi-scale characteristics (see Figure 5G): while the entire robot cluster operates on a meter scale, the geometrical features of the tentacles are less than 1 mm. Furthermore, the system exhibits temporal multi-scaling, with interactions ranging from high-frequency micro-collisions on a millisecond scale to macroscopic behaviors like shell formation and evaporation over several seconds. Traditional mechanical metamaterial designs typically consider only spatial multi-scaling. Our research demonstrates that by leveraging both spatial and temporal multi-scaling, architected particle robots achieve complex dynamic behaviors by incorporating bistability with high-frequency vibrations. This approach could spark innovative ideas in the field of mechanical metamaterials by exploring multi-scale behavior in space and time.

Furthermore, our exploration of these physical contact-based particle robots is not confined to specific sizes or materials. Figure 5H showcases a 3D model of microparticle robots, comparable in scale to a human cell, fabricated using a Nanoscribe.

This work underscores the scalability of our mechanism and highlights its potential applicability at the smaller scales. However, we acknowledge the technical challenges in testing and observing interactions at this scale, these remain promising areas for future exploration. This versatility in configurations, materials and fabrication scales dramatically expands the potential applications for these robots, opening up new possibilities in fields such as biomedical engineering, medical devices, and aerospace engineering.

Supporting Information

Supporting Information is available from the Wiley Online Library or from the author.

Acknowledgements

The authors thank Liane Makatura for proof reading the manuscript. This research was supported by start-up funding (grant no. DE00024892) from the Daniel Guggenheim School of Aerospace Engineering at the Georgia Institute of Technology

Conflict of Interest

The authors declare no conflict of interest.

Author Contributions

Xinyi Yang: investigation (lead); project administration (lead); validation (lead); visualization (lead); writing—original draft (lead); writing—review & editing (lead). **Bohan Wang**: formal analysis (equal); methodology (equal); software (equal); visualization (equa); writing—original draft (equal). **Víctor Riera Naranjo**: investigation (equal); visualization (equal); writing—review & editing (equal). **Minghao Guo**: investigation (equal). **Olivia Rivera**: investigation (supporting). **Leonid Sopizhenko**: investigation (supporting). **Shucong Li**: investigation (supporting); writing—original draft (supporting); writing—review & editing (supporting). **William Freeman**: conceptualization (lead); funding acquisition (equal); project administration (supporting); resources (equal). **Wojciech Matusik**: conceptualization (lead); funding acquisition (equal); resources (equal). **Bolei Deng**: conceptualization (lead); data curation (equal); formal analysis (equal); funding acquisition (equal); investigation (equal); methodology (lead); software (equal); supervision (lead); validation (equal); visualization (equal); writing—original draft (lead); writing—review & editing (lead). **Xinyi Yang** and **Bohan Wang** contribute equally to this work.

Data Availability Statement

The data that support the findings of this study are available in the supplementary material of this article.

Keywords

metamaterials, particle robots, physical intelligence

Received: February 4, 2025
Revised: April 29, 2025
Published online: July 14, 2025

[1] J. Kennedy, *Handbook of nature-inspired and innovative computing: Integrating classical models with emerging technologies*, Springer **2006**, 187.
[2] E. Bonabeau, M. Dorigo, G. Theraulaz, *Swarm intelligence: From natural to artificial systems*, Oxford university press **1999**.
[3] M. Brambilla, E. Ferrante, M. Birattari, M. Dorigo, *Swarm Intell.* **2013**, *7*, 1.
[4] S. Camazine, J.-L. Deneubourg, N. R. Franks, J. Sneyd, G. Theraula, E. Bonabeau, *Self-Organization In Biological Systems*, Princeton university press **2020**.
[5] S. Garnier, J. Gautrais, G. Theraulaz, *Swarm Intell.* **2007**, *1*, 3.
[6] I. Navarro, F. Mata, *ISRN Robot.* **2013**, *2013*, 1.
[7] A. E. Turgut, H. Çelikkanat, F. Gökçe, E. Sahin, *Swarm Intell.* **2008**, *2*, 97.
[8] E. Ferrante, A. E. Turgut, C. Huepe, A. Stranieri, C. Pinciroli, M. Dorigo, *Adapt. Behav.* **2012**, *20*, 460.
[9] C. Virágh, G. Vásárhelyi, N. Tarcai, T. Szörényi, G. Somorjai, T. Nepusz, T. Vicsek, *Bioinspir. Biomim.* **2014**, *9*, 025012.
[10] J. Pugh, A. Martinoli, in *2007 IEEE swarm intelligence symposium*, IEEE, **2007**, 332.
[11] H. Wei, Y. Cai, H. Li, D. Li, T. Wang, in *2010 IEEE Inter. Conf. on Robotics and Automation*, IEEE **2010**, 66.
[12] M. Dorigo, in *Proc. 2005 IEEE Swarm Intelligence Symp., 2005. SIS 2005.* IEEE, **2005**, 192.
[13] W. Savoie, T. A. Berrueta, Z. Jackson, A. Pervan, R. Warkentin, S. Li, T. D. Murphey, K. Wiesenfeld, D. I. Goldman, *Sci. Robot.* **2019**, *4*, eaax4316.
[14] D. H. Kim, H. Wang, S. Shin, *J. Intell. Robot. Syst.* **2006**, *45*, 369.
[15] Z. Kira, M. A. Potter, in *2009 4th Inter. Conf. on Autonomous Robots and Agents*, IEEE **2009**, 566.
[16] S. Li, R. Batra, D. Brown, H.-D. Chang, N. Ranganathan, C. Hoberman, D. Rus, H. Lipson, *Nature* **2019**, *567*, 361.
[17] M. Rubenstein, A. Cornejo, R. Nagpal, *Science* **2014**, *345*, 795.
[18] J. Chen, M. Gauci, W. Li, A. Kolling, R. Groß, *IEEE Trans. Robot.* **2015**, *31*, 307.
[19] M. Schranz, M. Umlauft, M. Sende, W. Elmenreich, *Front. Robot. AI* **2020**, *7*, 36.
[20] R. S. Parpinelli, H. S. Lopes, *Int. J. Bio-Ins. Comput.* **2011**, *3*, 1.
[21] A. Prorok, M. Malencia, L. Carlone, G. S. Sukhatme, B. M. Sadler, V. Kumar, *arXiv preprint arXiv:2109.12343* **2021**, 1.
[22] N. Hazon, G. A. Kaminka, in *Proc. of the 2005 IEEE international conference on robotics and automation*, IEEE **2005**, 735.
[23] Y. Tan, Z.-y. Zheng, *Def. Technol.* **2013**, *9*, 18.
[24] L. Bayindir, E. Sahin, *Turk. J. Elec. Eng. Comput. Sci.* **2007**, *15*, 115.
[25] R. Groß, M. Bonani, F. Mondada, M. Dorigo, *IEEE Trans. Robot.* **2006**, *22*, 1115.
[26] M. Yim, W.-M. Shen, B. Salemi, D. Rus, M. Moll, H. Lipson, E. Klavins, G. S. Chirikjian, *IEEE Robot. Autom. Mag.* **2007**, *14*, 43.
[27] M. Schranz, B. Rinner, in *Inter. Conf. on Sensor Networks*, SCITEPRESS **2015**, *2*, 15.
[28] M. Hartbauer, H. Romer, in *The First IEEE/RAS-EMBS Inter. Conf. on Biomedical Robotics and Biomechatronics, 2006. BioRob 2006*, IEEE **2006**, 585.
[29] D. Andréen, P. Jenning, N. Napp, K. Petersen, in *ACADIA 2016 ("Posthuman Frontiers: Data, Designers, and Cognitive Machines"), 36th Annual Conf. of the Association for Computer Aided Design in Architecture*, Association for Computer-Aided Design in Architecture (ACADIA), Ann Arbor, Michigan, USA **2016**, 54–61.
[30] M. Nisser, Y. Makaram, F. Faruqi, R. Suzuki, S. Mueller, in *2022 IEEE/RSJ Inter. Conf. on Intelligent Robots and Systems (IROS)*, IEEE **2022**, 12659.
[31] Y. Liu, X. Zhang, *Chem. Soc. Rev.* **2011**, *40*, 2494.
[32] T. J. Cui, D. R. Smith, R. Liu, *Metamaterials*, Springer **2010**.

[33] R. Kumar, M. Kumar, J. S. Chohan, S. Kumar, *Mater. Today Proc.* **2022**, *56*, 3016.
[34] S. Babaee, J. Shim, J. C. Weaver, E. R. Chen, N. Patel, K. Bertoldi, *Adv. Mater* **2013**, *25*, 5044.
[35] H. Yasuda, J. Yang, *Phys. Rev. Lett.* **2015**, *114*, 185502.
[36] D. Mousanezhad, S. Babaee, H. Ebrahimi, R. Ghosh, A. S. Hamouda, K. Bertoldi, A. Vaziri, *Sci. Rep.* **2015**, *5*, 18306.
[37] N. Vasios, B. Deng, B. Gorissen, K. Bertoldi, *Nat. Commun.* **2021**, *12*, 695.
[38] L. Jin, R. Khajehtourian, J. Mueller, A. Rafsanjani, V. Tournat, K. Bertoldi, D. M. Kochmann, *Proc. Natl. Acad. Sci.* **2020**, *117*, 2319.
[39] X. Zhang, H. Ye, N. Wei, R. Tao, Z. Luo, *Mater. Des.* **2021**, *209*, 109990.
[40] B. Deng, P. Wang, Q. He, V. Tournat, K. Bertoldi, *Nat. Commun.* **2018**, *9*, 3410.
[41] B. Deng, J. Li, V. Tournat, P. K. Purohit, K. Bertoldi, *J. Mech. Phys. Solids* **2021**, *147*, 104233.
[42] B. Jenett, C. Cameron, F. Tourlomousis, A. P. Rubio, M. Ochalek, N. Gershenfeld, *Sci. Adv.* **2020**, *6*, eabc9943.
[43] B. Deng, A. Zareei, X. Ding, J. C. Weaver, C. H. Rycroft, K. Bertoldi, *Adv. Mater* **2022**, *34*, 2206238.
[44] D. Haver, D. Acuña, S. Janbaz, E. Lerner, G. Düring, C. Coulais, *Proc. Natl. Acad. Sci.* **2024**, *121*, e2317915121.
[45] T. Chen, M. Pauly, P. M. Reis, *Nature* **2021**, *589*, 386.
[46] A. Djellouli, B. Van Raemdonck, Y. Wang, Y. Yang, A. Caillaud, D. Weitz, S. Rubinstein, B. Gorissen, K. Bertoldi, *Nature* **2024**, 1.
[47] M. C. Göpfert, H. Briegel, D. Robert, *J. Exp. Biol.* **1999**, *202*, 2727.
[48] S. Foy, *The grand design: form and colour in animals*, Prentice Hall **1983**.
[49] T. L. Lentz, *J. Gen. Virol.* **1990**, *71*, 751.
[50] M. S. Maginnis, *J. Mol. Biol.* **2018**, *430*, 2590.
[51] J. Schneider-Schaulies, *J. Gen. Virol.* **2000**, *81*, 1413.
[52] M. A. Chowdhury, M. Helali, *Tribol. Int.* **2008**, *41*, 307.
[53] M. Asaduzzaman Chowdhury, M. Helali, *Ind. Lubr. Tribol.* **2009**, *61*, 154.
[54] P. Wang, H. Ni, R. Wang, Z. Li, Y. Wang, *Tribol. Int.* **2016**, *99*, 237.
[55] P. Wang, H. Ni, R. Wang, W. Liu, S. Lu, *Materials* **2017**, *10*, 1015.
[56] C. Scholz, M. Engel, T. Pöschel, *Nat. Commun.* **2018**, *9*, 931.
[57] Z. Hao, S. Mayya, G. Notomista, S. Hutchinson, M. Egerstedt, A. Ansari, *IEEE Trans. Robot.* **2022**, *39*, 590.